RESEARCH ARTICLE OPEN ACCESS

Single-Hole Charging in Self-Assembled Silicon Nanostructures

N.T. Bagraev*, A.D. Bouravleuv*, V.S. Khromov*, L.E. Klyachkin*, A.M. Malyarenko*, W. Gehlhoff**, S.A. Rykov***

**(Department of Atomic Radiospectroscopy, Ioffe Institute, St. Petersburg, Russia*
*** (Institut fűr Festkörperphysik, TU Berlin, Berlin, Germany*
****(Department of Semiconductor Physics and Nanoelectronics, Peter the Great St. Petersburg Polytechnical University, St. Petersburg, Russia*

ABSTRACT
Firstly, we present ultra-shallow (5-30 nm) diffusion profiles performed by short-time boron diffusion from the gas phase into the n-type Si(100) wafer using controlled surface injection of self-interstitials and vacancies. The diffusion profiles of this art are found to consist of both self-assembled longitudinal and lateral quantum wells formed naturally between the δ - barriers heavily doped with boron. Secondly, the recharging of many-hole and few-electron quantum dots under the conditions of the ballistic transport of single charge carriers inside self-assembled quantum well structures on a Si (100) surface are studied using local tunneling spectroscopy at high temperatures (up to room temperature). On the basis of measurements of the tunneling current–voltage characteristics observed during the transit of single charge carriers through charged quantum dots, the modes of the Coulomb blockade, Coulomb conductivity oscillations, and electronic shell formation are identified. Finally, the tunneling current–voltage characteristics also show the effect of quantum confinement and electron–electron interaction on the characteristics of single-carrier transport through silicon quantum wires containing weakly and strongly coupled quantum dots.
Keywords: silicon quantum well, wire, dot, Coulomb blockade, artificial atom, weak and strong coupling

I. INTRODUCTION

The fabrication of semiconductor structures with self-assembled quantum wells (QWs) and superlattices is one of the most important problems of modern semiconductor physics and nanoelectronics. In recent years, this problem has become especially important in the context of the need to create fundamentally new nanoelectronic and optoelectronic devices, such as single electron transistors, single-electron memory cells, and lasers that operate via intraband transitions [1–4]. Accordingly, the development of new technologies for semiconductor nanostructures raises an increasingly greater number of questions related to the microscopic nature of self-assembled QWs and the two-dimensional barriers separating them, as it is upon these that the fabrication of quantum wires (QWrs) and quantum dots (QDs) using the electrostatic confinement of charge carrier motion is based.

QDs are zero-dimensional systems that are obtained by fully confining the motion of charge carriers in QWrs, QWs, or in bulk crystals. Since the charge carriers in a QD are confined in all directions, the corresponding energy spectrum is completely discrete, just as it is for an isolated atom. For this reason, QDs are often called artificial atoms, although each QD consists of thousands, or even hundreds of thousands, of real atoms. Naturally, in this case, charged QDs are implied. Empty QDs cannot be considered as analogues of real atoms, but they are of special interest for studying charge-carrier resonant tunneling through zero-dimensional systems [5]. In turn, like a real atom, a charged QD (an artificial atom) can contain one or several free charge carriers exhibiting confinement effects and the effects of electron–electron interaction during recharging. The relative contributions of these effects are determined by the dot size and by the characteristics of its boundary [2, 6].

Like QWs and QWrs, QDs can be obtained both using molecular-beam epitaxy in combination with nanolithography and selective etching [1, 2, 6, 7] and electrostatically using deposited metal microcontacts [2, 8]. In the first case, taking AlGaAs/GaAs as an example, the formation of QDs inside the heterostructure starts from the deposition of masks onto the surface of the wide-gap semiconductor (AlGaAs). Then, the entire AlGaAs layer and part of the GaAs layer are removed by deep etching. Electrons produced by ionization of the shallow donor centers in AlGaAs concentrate in the zero-dimensional GaAs dots that appear. Therefore, the number of charge carriers localized in a QD is determined by the donor concentration and by the self-compensation resulting from the formation of DX centers [9]. This self-compensation gives rise to a lot of problems in the study of ballistic carrier transport, but the disadvantage can be eliminated by applying an electrostatic method in which one-dimensional and zero-dimensional systems are created by confining the motion of the

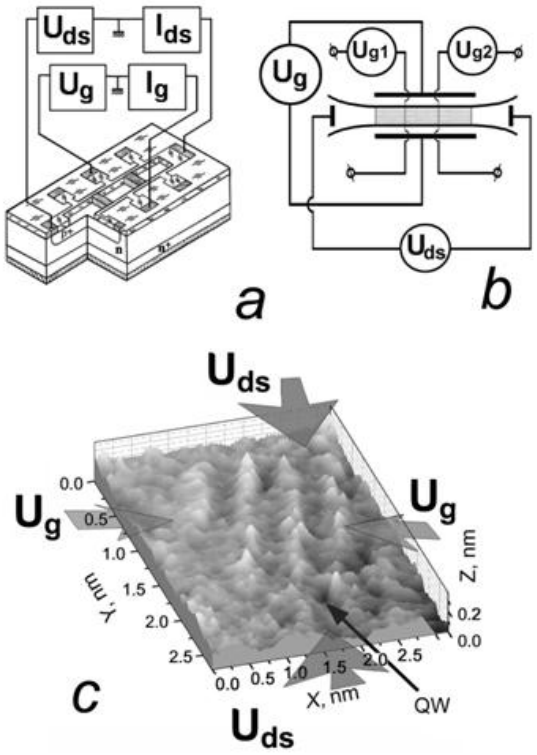

Fig. 1. (a) A planar p^+–n structure with Hall geometry (schematic diagram). The structure is designed for studying the Coulomb blockade, Coulomb oscillations, and Coulomb staircase of quantum dot conductance during the transport of individual charge carriers. (b) A schematic representation of the split-gate (U_g) used for inducing modulated QWrs inside QWs. The voltages U_{g1} and U_{g2} are applied to the finger gates intended for producing quantum dots. (c) A 3D split-gate image obtained by scanning tunneling microscopy in the vicinity of a QW on the Si (100) surface.

charge carriers in QWs (Figs. 1a, 1b). The main advantage of this method is that it makes it possible to increase the number of electrons or holes in a QD to several hundred, thus allowing the observation of certain interesting phenomena such as the Coulomb blockade and Coulomb oscillations arising due to the enhancement of the electron–electron interaction [2, 8].

One of the unresolved problems of practical nanoelectronics consists in finding the relative contributions made by quantum interference and electron–electron interaction to the ballistic transport in electrostatically induced QWrs under the conditions of the elastic back-scattering of charge carriers by internal δ-shaped barriers. This type of modulation in the coherent transport of single charge carriers can occur as a result of the effect of residual impurity centers distributed over the boundaries of a QWr and also due to a nonuniform distribution of the gate voltage along this QWr [10, 11]. By varying the source–drain voltage (U_{ds}) and the gate voltage (U_g), we can not only enhance the effect of the random electrostatic δ-barriers but also create a QD inside the QWr using the split-gate technique. The transport characteristics of the QD are controlled by finger gates, whereas the central gate voltage controls the number of charge carriers in the QD (Fig. 1). Thus, an electrostatically generated charged QD represents an artificial atom. Moreover, it is possible to change the number of charge carriers in this atom using an external electric field.

The characteristics of the QDs inside QWs can be monitored by local tunneling spectroscopy (Fig. 2a). In this case, the voltage U_{tunn} applied between the tip of the scanning tunneling microscope (STM) and the point of contact at the boundary of the planar structure, which is equal to the potential difference between the ends of an electrostatically induced quantum wire and is the sum of the source–drain voltage and the gate voltage, is

$$U_{tunn} = U_{ds} + U_g \quad (1)$$

Depending on the number of charge carriers in a QD, we can distinguish between many-electron and few-electron artificial atoms. It should be noted that the number of charge carriers determines the effects that can be observed in relation to ballistic transport. For example, the Coulomb oscillations in the conductivity that appear when changing the central

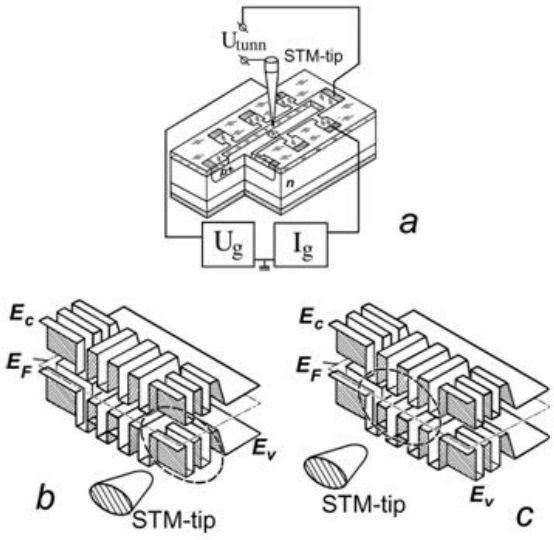

Fig. 2. (a) A planar structure containing a p+ diffusion profile with an approaching tunneling microscope tip. (b, c) 3D band diagrams of a longitudinal p-type QW at the n-Si surface, which contains a quantum dot representing a multitunneling junction under the conditions (b) $U_{tunn} = U_{ds}$ and (c) $U_{tunn} = U_g$. The dashed circle shows the region of the point of contact of the tip.

gate voltage (Fig. 1a) are exclusively of a many-electron character [6, 8]. Few-electron QDs, however, exhibit many properties typical of real atoms, such as orbital degeneracy and shell formation [12, 13]. In addition, the detection of the Kondo effect and Fano resonances in low-dimensional systems containing few-electron QDs provides yet more evidence of the similarity between real and artificial atoms [14, 15].

In this study, we use local tunneling spectroscopy to investigate different modes of the ballistic transport of single holes through many-electron and few-electron QDs inside self-assembled QWs on a Si (100) surface. We focus on the detection of one-hole recharging at high temperatures (up to room temperature). The detection is carried out using a connected series of several QDs with a capacitance of ~10^{-19} F.

In the following sections, the characteristics of p-type silicon QWs formed between self-assembled layers of microdefects, which were obtained by a preliminary oxidation and subsequent boron diffusion on a Si (100) surface, are briefly analyzed. We present data obtained from studies of the effects of Coulomb oscillations and the Coulomb blockade. These effects arise during the single-hole recharging of a QD, which is electrostatically induced inside a QWr using a split gate built into the plane of the self-assembled Si QWs (SASQWs). Next, the local tunneling spectra, showing the effects of the Coulomb blockade and Coulomb oscillations when a single hole travels through weakly coupled many-electron QDs inside the SASQW structures (SASQWSs), are discussed. Finally, the corresponding tunneling current–voltage characteristics of strongly coupled few-electron QDs are described. These characteristics indicate various scenarios for electronic shell formation that depend on the number of electrons in a QD and on its shape.

II. SELF-ASSEMBLED SILICON QUANTUM WELLS

It is known that the formation of oxide layers on the surface of monocrystalline Si facilitates the generation of excess fluxes of intrinsic interstitial atoms and vacancies. Moreover, it is known that these fluxes have a preferential crystallographic direction along the ⟨111⟩ and ⟨100⟩ axes, respectively [16–19]. At the initial stage of oxidation, the formation of a thin oxide layer is accompanied by the generation of excess interstitial Si atoms, which can form small microdefects, whereas the fluxes of vacancies in the opposite direction result in the annihilation of these defects (Fig. 3a). Since the sources and sinks of excess interstitial atoms and vacancies on the oxidized Si(100) surface are located close to positively and negatively charged reconstructed silicon dangling bonds, respectively [19], it can be assumed that the size of the microdefects, consisting of intrinsic interstitial atoms and pyramidal in shape, is about 2 nm. Therefore, the distribution of the microdefects created at the initial stage of oxidation apparently represents a modification of a Sierpinski gasket-type fractal and includes a built-in longitudinal QW (Figs. 3b and 4a).

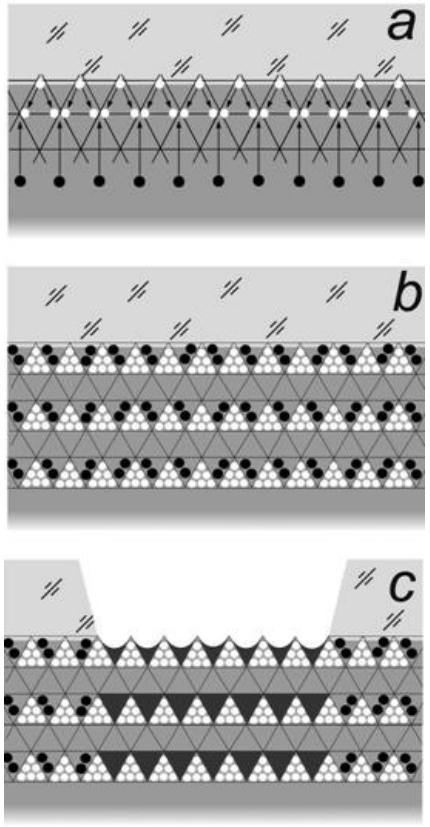

Fig. 3. Diagrams illustrating the fabrication of a self-assembled silicon quantum well structure (SASQWS) on the Si (100) surface under the conditions of injection of intrinsic interstitial Si atoms (open circles) and vacancies (filled circles) during (a, b) preliminary oxidation and (c) subsequent boron diffusion: (a) The excess fluxes of intrinsic interstitial Si atoms and vacancies that are generated during preliminary oxidation of the Si (100) surface and are crystallographically oriented along the [111] and [100] axes, respectively. (b) A diagram of a longitudinal SASQWS that appears between the layers of the microdefects formed from intrinsic interstitial Si atoms and vacancies at the stage of preliminary oxidation of the Si (100) surface. (c) A diagram of a longitudinal SASQWS formed by the subsequent passivation of the microdefects by the vacancy mechanism (dark regions) under the conditions of a short period of boron diffusion using planar silicon technology.

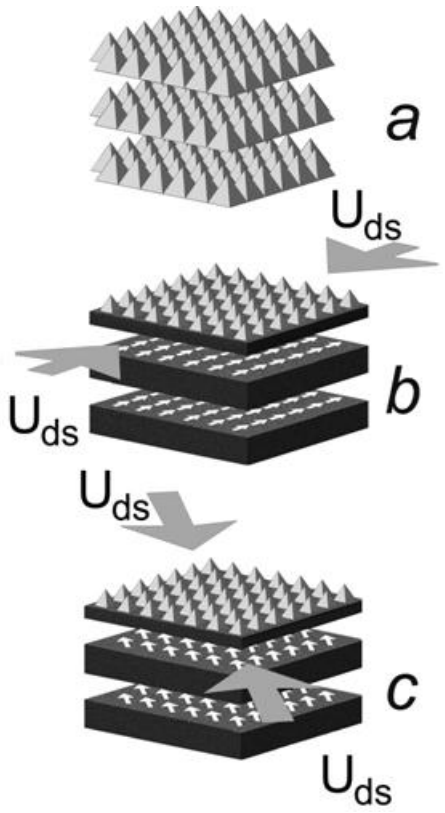

Fig. 4. A 3D image of the longitudinal SASQWSs (a) formed between the layers of microdefects, which are then (b, c) transformed into neutral δ barriers after passivation by the vacancy mechanism under a short period of boron diffusion. The white arrows show the direction of the ordering of the boron impurity dipoles inside the δ barriers under the conditions of a source–drain voltage U_{ds} applied along the crystallographic axes (b) [001] and (c) [011].

It should be noted that, during further oxidation of the Si (100) surface, the fractal distribution of the microdefects is reproduced and the dimensions of separate microdefects nucleated at Pb centers [20] increase [21]. However, the growth of thick oxide layers results in the predominant generation of vacancies by the oxidized surface and, hence, to the disappearance of microdefects and the self-assembly of transverse QWs [10, 21].

Although the structures of both the longitudinal and transverse silicon QWs introduced into the fractal system of microdefects are of great interest in relation to their use as a basis for optically and electrically active microcavities in optoelectronics and in relation to nanoelectronics, the presence of dangling bonds at their boundaries is a deleterious factor for the practical implementation of such structures. Therefore, in order to passivate dangling bonds and other defects created during the preliminary oxidation of Si (100) substrates, it is reasonable to implement a subsequent short period of boron diffusion, which can transform the layers of microdefects into neutral δ-shaped barriers bounding the SASQWSs (Figs. 3c, 4b, and 4c).

To this end, we used *n*-Si (100) substrates that were 0.35 mm thick and had resistivities of 500 and 20 Ohm cm. The substrates were preliminarily oxidized at a temperature of 1150°C in an atmosphere of dry oxygen containing CCl_4 vapors. The thickness of the oxide layers depended on the oxidation time, which was varied from 20 min to 24 h. Below, for the purposes of the fabrication and study of longitudinal SASQWSs, we mainly focus on samples with a thin oxide layer (0.22 μm), in which windows in the Hall geometry were formed photolithographically in order to perform a short period of boron diffusion from the gas phase at T_{dif} =900°C. It is known that, at this temperature, an equilibrium between different diffusion mechanisms is established [10, 16–18]. This equilibrium results in a sharp retardation of the rate at which boron is diffused into silicon and facilitates the optimum passivation of the layers of microdefects bounding the SASQWSs (Figs. 3c, 4b, and 4c). It should be noted that the pyramidal microdefects consisting of intrinsic interstitial atoms, which become apparent at the stage of chemical etching [18], did not disappear after the short period of boron diffusion (Fig. 1c).

An earlier analysis of the resulting ultra-shallow boron concentration profiles using secondary-ion mass spectrometry (SIMS) [22] has shown that their depth does not exceed 7 nm [10, 17, 18, 21]. Thus, the depth of the diffusion profiles virtually corresponds to the expected vertical size of the self-assembled silicon nanostructure consisting of longitudinal SASQWSs bounded by δ-shaped barriers (Figs. 3c, 4b, and 4c). In addition, the presence of a *p*-type QW at the *n*-Si (100) surface was verified by the four-probe method under the conditions of layer-by-layer etching. The application of SIMS to this verification encountered certain difficulties related to the limited resolution of this method and to the smoothing of the ultra-shallow diffusion profile as a result of the diffusion of impurity atoms under the action of an ionic beam [17, 18].

Figs. 5 a, b and c show the important role of back side oxidation in determining the diffusion profile depth for the kick-out and vacancy diffusion mechanisms. Since the diffusion process proceeds at 800°C and 1100°C respectively via the vacancy and the kick-out mechanisms, the smallest penetration depths were observed in the case of both the suppression of excess fluxes and annihilation of self-interstitials and vacancies near the back side (see curves 1,3 in Figs. 5 a, c). The diffusion profile depth

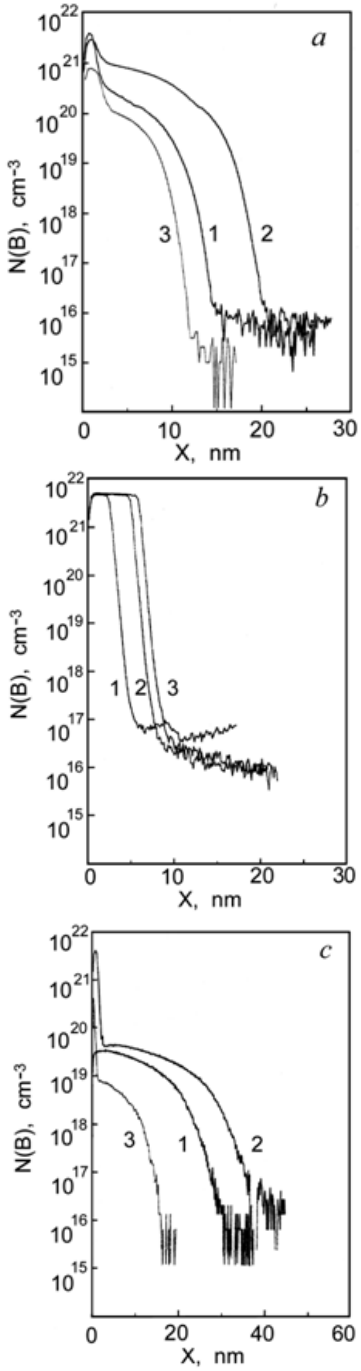

Fig. 5. SIMS data for boron diffusion profiles obtained at diffusion temperatures of 800°C (a), 900°C (b) and 1100°C (c) into the Si(100)-wafers of the n-type ($N(P)=2x10^{14}cm^{-3}$) with a thin (curves 1), medium (curves 2) and thick (curves 3) oxide overlayer.

is seen to reach the maximum at the diffusion temperature of 800°C and 1100°C in the presence of medium oxide overlayer on both the working and back side of the Si(100) wafer (see curves 2 in Figs. 5 a, c) that is in a good agreement with the scheme in Fig. 3.

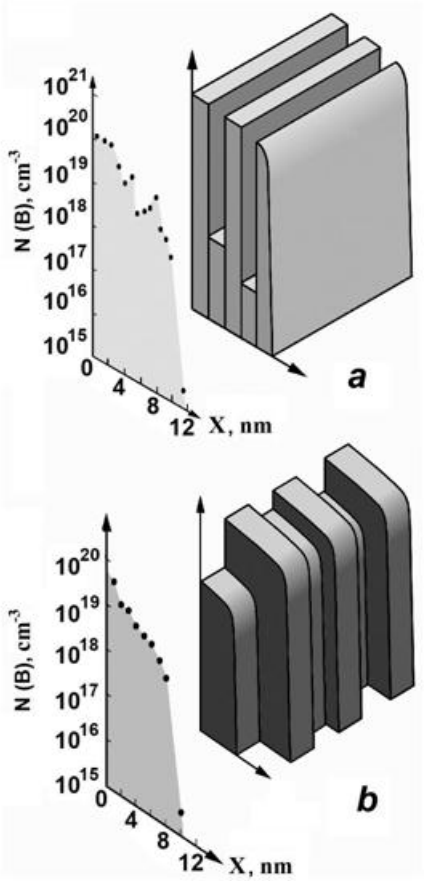

Fig. 6. Ultra-shallow boron diffusion profiles into the Si (100) wafer of the n-type which are prepared at the diffusion temperature of 900°C (a) and 800°C (b) and analyzed by the four-point probe method using the technique of layer-by-layer etching, and corresponding models of the diffusion profiles obtained that consist of longitudinal and lateral quantum wells respectively parallel and perpendicular to the p^+-n junction plane.

The retardation of the diffusion process that occurs under parity between the kick-out and vacancy diffusion mechanisms is found to be revealed also by varying the diffusion temperature thereby minimizing the diffusion profile depth at 900°C (Fig. 5 b). The analysis of this diffusion profile by the four-point probe method using layer-by-layer etching demonstrates the deviations in the distribution of the concentration of the dopant (Fig. 6 a), whereas the ultra-shallow boron profile obtained by the vacancy diffusion mechanism at 800°C is practically smooth (Fig. 6 b). The different shape of the diffusion profiles studied seems to be a consequence of self-assembled longitudinal (Figs. 6 a) and lateral (Fig. 6 b) quantum wells (SQW) that are identified in such structures by the cyclotron resonance (CR) angular dependencies [21]. These CR measurements were performed at 3.8 K with an EPR spectrometer at X- band (9.1-9.5

GHz). The rotation of the magnetic field in a plane normal to the diffusion profile plane has revealed the anisotropy of both the electron and hole effective masses in silicon bulk and Landau levels scheme in SQW. This CR quenching and the line shifts for which a characteristic 180^o symmetry was observed can be explained with the effect of the electrical field created by the confining potential inside p+-diffusion profile and its different arrangement in longitudinal and lateral SQW formed naturally between the δ barriers heavily doped with boron. The results obtained exhibit the longitudinal SQW into the diffusion profiles prepared at 900°C (Fig. 6 a), while the lateral SQW cross the 800°C structures (Fig. 6 b) [21, 23].

Space-independent excess fluxes of intrinsic defects that cause the formation of SQW appear to be transformed also into microdefects which can be revealed by the STM technique as the deformed potential fluctuations (DPF) near the $Si\text{-}SiO_2$ interface and the surface of the ultra-shallow diffusion profile. The DPF effect induced by the microdefects of the self-interstitials type that are displayed as light poles in Figs. 7 and 8 is demonstrated to be brought about by the previous oxidation and to be enhanced by subsequent boron diffusion (Fig. 7). The STM technique allowed to define crystallographic orientation of DPF obtained by using thick (Fig. 8a) and thin (Fig. 8b) oxide

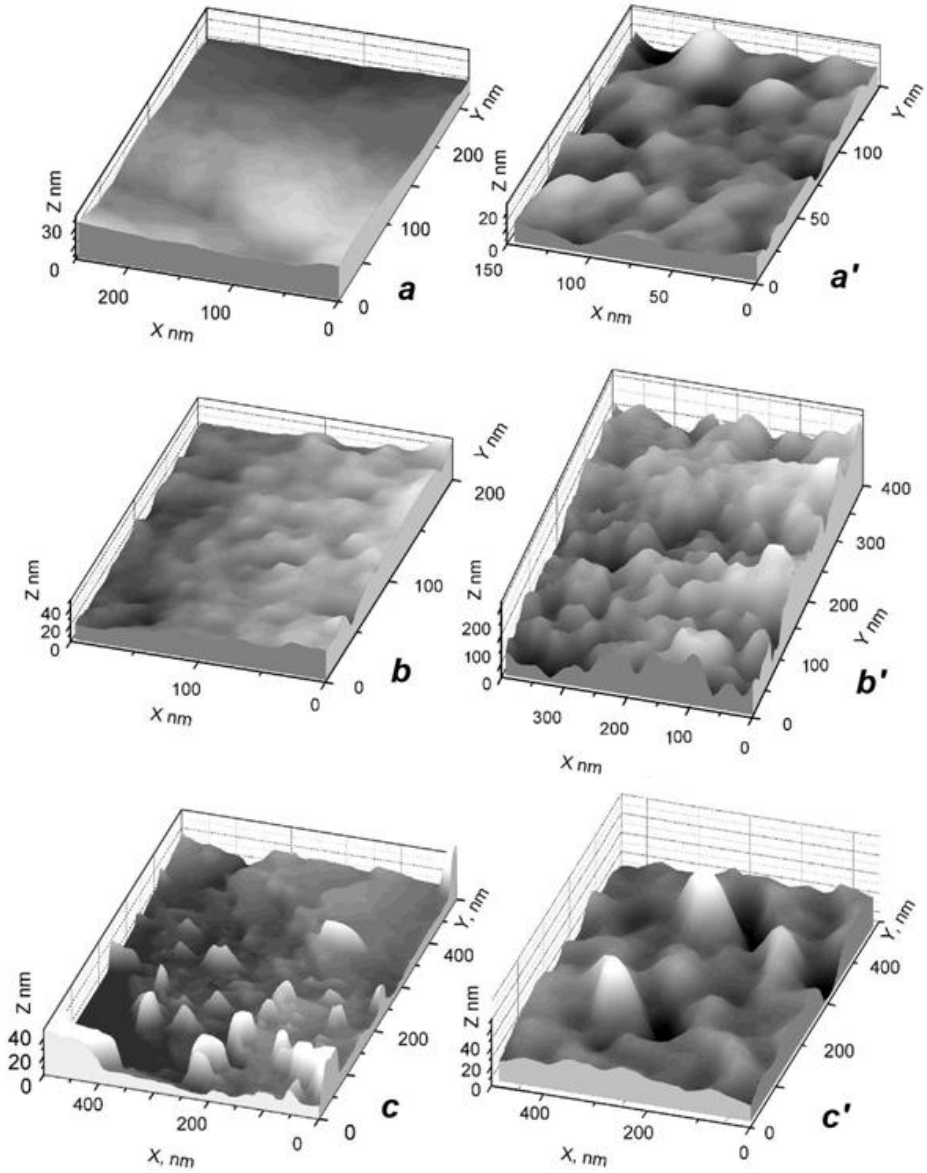

Fig. 7. STM images of the $Si\text{-}SiO_2$ interface windows after etching medium (a), thin (b) and thick (c) oxide overlayer and ultra-shallow boron diffusion profiles into the same windows which were prepared at diffusion temperature of 1100°C (a') and 800°C (b' and c'). X||[001], Y||[010], Z||[100].

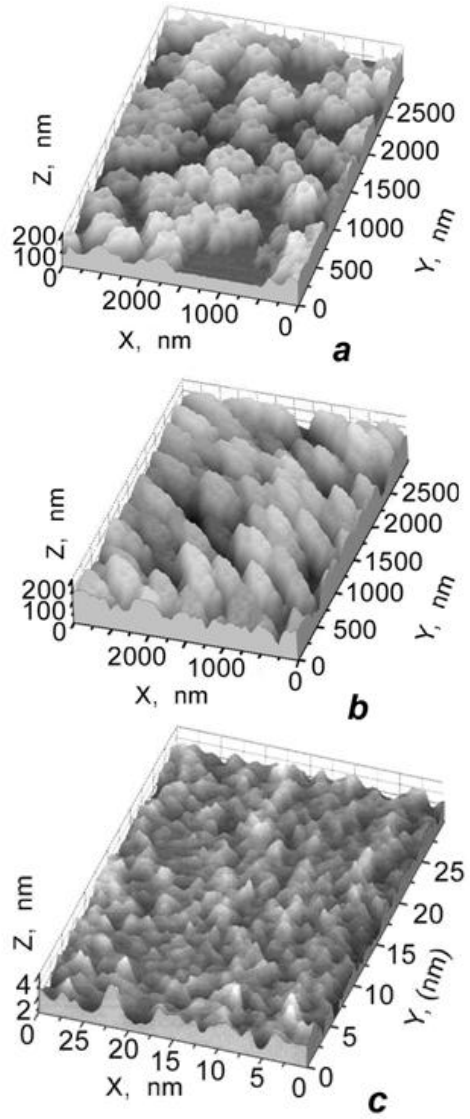

Fig. 8. STM images of the ultra-shallow boron diffusion profiles prepared at diffusion temperature of 800°C (a and b) and 900°C (c) into the Si(100) wafer covered previously by thick (a), thin (b) and medium (c) oxide overlayer. X||[001], Y||[010], Z||[100].

overlayer that corresponds respectively to a <100> and <111> axis and visualizes practically the orientation of excess fluxes of self-interstitials as a function of the oxide overlayer thickness. The analysis of the STM image of the ultra-shallow boron profile prepared under parity conditions between diffusion mechanisms (Fig. 8c) enables to hazard a conjecture that the dimension of the microdefect observed is consistent with the parameters expected from the tetrahedral model of the Si_{60} cluster [24]. Thus, the DPF effect gives rise to the formation of self-assembled quantum antidots with dimensions that are equalized as the diffusion temperature increases. Besides, the interplay between the dimensions of these antidots and their distribution inside the ultra-shallow diffusion profile prepared on the Si(100) wafer is found to be evidence of the fractal mechanism that causes the formation of the self-assembled zero-dimensional systems because of strong coupling between the excess fluxes of intrinsic defects and dopants. Finally, self-assembled quantum antidots embedded into the SQW system are shown to be the microcavities (Fig. 9a) [25] that exhibit a distributed feedback identified by the Rabi splitting as well as the photoluminescence from SQW and residual impurity center, which are revealed by the spectral dependencies of transmission coefficient (Fig. 9 b and c).

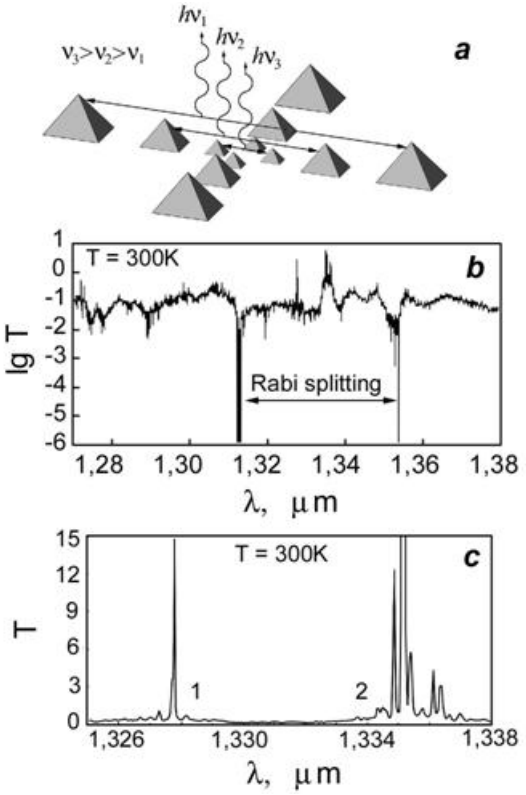

Fig. 9. (a)- The model of the self-assembled microcavity system formed by antidots that are caused by the fractal impurity diffusion using excess fluxes of intrinsic defects.
(b), (c) – Spectral dependence of the light transmission coefficient through self-assembled antidot system which identifies the microcavities embedded into the ultra-shallow p^+-diffusion profile prepared on the Si (100) wafer (b) that are able to enhance the photoluminescence due to the optical transitions between quantum-dimensional subbands that belong to a self-assembled quantum well and intrinsic photoluminescence caused by residual impurity center, which are embedded into self-assembled quantum well (c).

The characteristics of the single *p*-type SAQW were determined from the angular dependence of the cyclotron resonance of electrons and holes when the magnetic field was rotated in the {110} plane perpendicular to the plane of the boron diffusion profile on the Si (100) surface [23, 26]. The quenching and shift of the cyclotron resonance lines recorded by an ESR spectrometer (*X*-band, 9.1–9.5 GHz) were found to show a 180° symmetry when the magnetic field was oriented parallel to the plane of the obtained ultra-shallow boron profile, which clearly indicated that the QW was oriented parallel to the (100) planes.

The cyclotron resonance spectra (Fig. 10) consist of unusually narrow lines, indicating a substantial increase in the spin–lattice relaxation time of the non-equilibrium electrons and holes in the SASQWSs as compared to the corresponding times for the bulk Si samples. The relaxation times estimated from the width of the cyclotron resonance spectral lines for the electrons ($\tau \approx 7\times10^{-10}$ s), light holes ($\tau \approx 5\times10^{-10}$ s), and heavy holes ($\tau \geq 5\times10^{-10}$ s) directly indicate a high mobility of two-dimensional charge carriers: $\mu \geq 200$ m^2/(V s). This result is rather unexpected in view of the boron doping level of the δ-shaped barriers between which the QWs are formed. In order to explain this fact, we used ESR data, which indicates that heavily doped δ-shaped barriers have ferroelectric properties, since they consistof trigonal impurity B^+–B^- dipoles [10, 27]. In this model, the reconstruction of shallow boron acceptors, resulting in the formation of neutral dipole centers ($2B_0 \rightarrow B^- + B^+$), must be accompanied by the appearance of a correlation energy gap in the density of states of the degenerate two-dimensional hole gas. The determination of this energy gap from the temperature dependence of the Seebeck

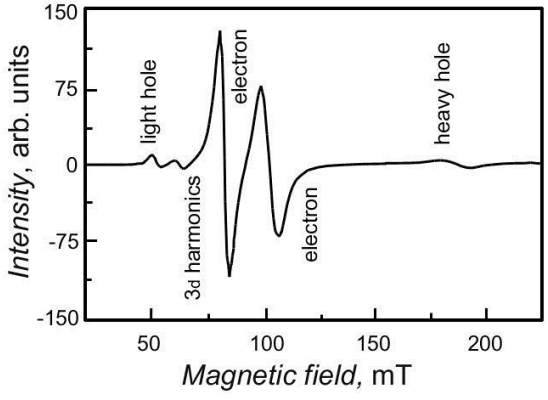

Fig. 10. The cyclotron resonance spectrum for a *p*-type SASQWS formed between the δ barriers at the *n*-Si (100) surface. The magnetic field is directed perpendicularly to the SASQWS planes in the plane {110}: $B \parallel \langle 100\rangle + 30°$. $T = 4.0$ K and $\nu = 9.45$ GHz.

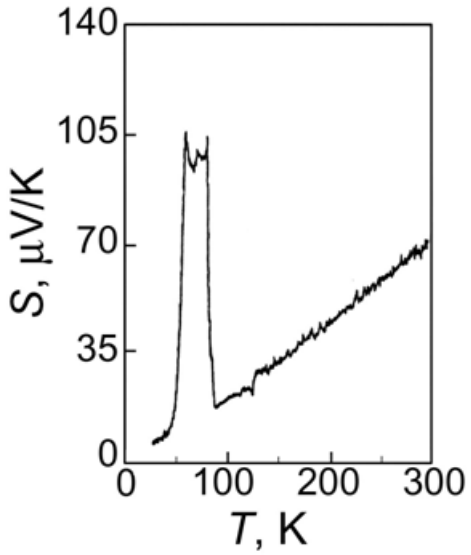

Fig 11. The temperature dependence of the thermoelectric power (Seebeck coefficient) for a *p*-type SASQWS formed between the δ barriers at the *n*-Si (100) surface.

coefficient (Fig. 11) makes it possible to explain the above values of the charge carrier mobility, which are retained in SASQWSs up to 77 K [28].The electrostatic ordering of the reconstructed impurity dipoles inside the δ-shaped barriers by an external electric field applied along different crystallographic axes in the plane of the SASQWSs (Figs. 4b, 4c) creates a transverse confinement of the charge carriers, which, it would seem, results in the angular dependence of the conductivity (Fig. 12). The conductivity maxima observed when the external electric field is oriented along the [010], [001], and [011] axes correspond to the crystallographic directions that are most energetically favorable for a reconstructed deep

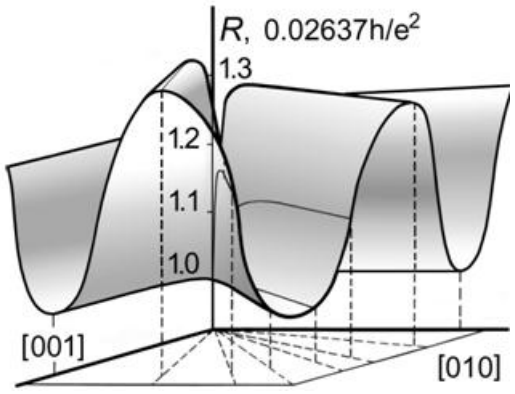

Fig. 12. The crystallographically dependent change in the resistance in the plane of a *p*-type SASQWS formed between the δ barriers at the *n*-Si (100) surface ($T = 77$ K).

center under the conditions of the quadratic Stark effect [29, 30]. Therefore, the presence of δ-shaped barriers with ferroelectric properties allows, in particular, the observation of a quantum conductivity staircase using a split-gate configuration (Fig. 1) both at zero and nonzero gate voltages [10, 31]. Furthermore, the electrostatic ordering of impurity dipoles, which gives rise to the transverse confinement of charge carriers moving along the plane of the QWs, allows us to use local tunneling spectroscopy to study quasi-one-dimensional charge carrier transport. In this case, the external electric field $U_{tunn} = U_{ds} + U_g$ applied in the plane of the QWs (Fig. 2a), on the one hand, gives rise to transverse confinement due to the ordering of the impurity dipoles (U_g) and, on the other hand, is responsible for the transport of individual charge carriers (U_{ds}).

III. MANY-ELECTRON ARTIFICIAL ATOMS

3.1. The Coulomb blockade and Coulomb oscillations

Figures 13a and 13b show the current–voltage (*I*–*V*) characteristics of a QD formed in an SASQWS using the split-gate technique (Fig. 1c). The dependence $I_{ds} = f(U_g)$ was measured at a small potential difference U_{ds} between the source and the drain, which only slightly exceeded the value required for the measurement of the tunneling conductivity between them. Nevertheless, the value of U_{ds} was sufficient for the formation of a one-dimensional channel in the SASQWS because of the electrostatic ordering of the impurity dipoles inside the δ-shaped barrier. In this case, it is not necessary to use finger gates, since the split-gate voltage is entirely localized at a QD formed near a pair of unreconstructed impurity dipoles [10]. Depending on the gate voltage, the current oscillates with a characteristic period that corresponds to the voltage required for introducing one charge carrier into the QD [6, 8]. Therefore, the Coulomb oscillations shown in Fig. 13a represent the current–voltage curve of a single-electron transistor that operates by "switching" the QD on and off each time a single charge carrier enters the QD in the process of quasi-one-dimensional transport.

The behavior of Coulomb oscillations can be considered using a model of the Coulomb blockade that arises under the conditions of weak coupling between the QD and the QWr containing it [32, 33]. This model describes the recharging mechanism of the QD during carrier tunneling through it inside the QWr; again, the QD is assumed to be electrically neutral. The energy required for introducing the charge *Q* into the QD is $Q^2/2C$, where

$$C = C_L + C_R + C_g \qquad (2)$$

is the total capacitance of the QD, C_L and C_R are the capacitances between the QD and the QWr containing it, and C_g is the gate capacitance (Figs. 14a, 14b). Since the minimum charge added to the QD corresponds to the charge of a single electron (hole), it follows that, for the current to flow through it, the energy $e^2/2C$ is required. Thus, charge quantization produces an energy gap e^2/C in the spectrum of the QD states (Figs. 14b, 14c). If the temperature is fairly low, i.e., if $kT < e^2/2C$, neither an electron nor a hole can tunnel inside the QWr containing the QD; i.e., we have a situation corresponding to the Coulomb blockade.

By varying the gate voltage U_g, we can change the energy required for adding charge to the QD (Fig. 14b). In this case, the gate voltage U_g is applied between the gate and the source. However, if the voltage between the source and the drain is very small, then the drain, the source, and the QD have the same potential. Therefore, in the presence of voltage at the gate, the electrostatic energy of the QD is changed [6, 8]:

$$E = QU_g + \frac{Q^2}{2C} \qquad (3)$$

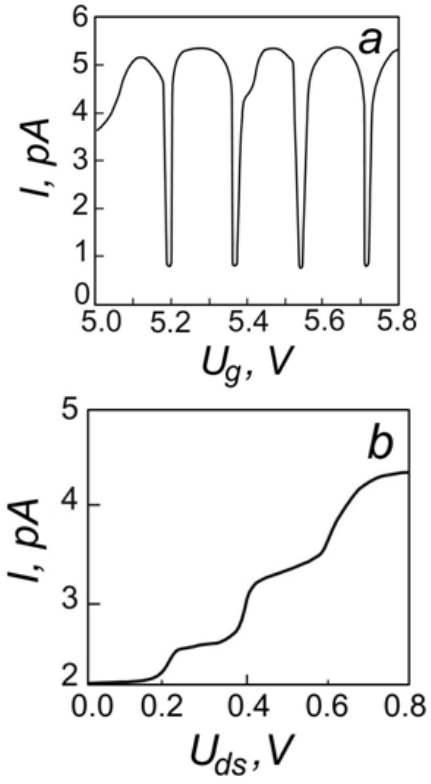

Fig. 13. (a) Coulomb oscillations and (b) the Coulomb staircase observed during the transit of single holes through a weakly coupled quantum dot inside a QWr formed using the split-gate technique in the plane of a *p*-type SASQWS formed between the δ barriers at the *n*-Si (100) surface (T = 77 K).

$$E = QU_g + \frac{Q^2}{2C} \quad (3)$$

In the case of a negative charge Q, the first term in the equation describes the attractive interaction between the charge Q and the positively charged gate, and the second term describes the electrostatic repulsion between the particles inside the QD. Equation (3) shows that the energy is at a minimum at $Q_0 = -C_gU_g$. By changing U_g, we can choose any value of Q_0 that minimizes the energy in Eq. (3) if the charge is not quantized. However, since the real charge is quantized, the variation in energy is discrete. As $Q_0 = -Ne$, the total number of charge carriers N corresponds to the minimum of the energy E, and the Coulomb interaction induces changes in the energy $e^2/2C$ as N either increases or decreases by unity. For any other value of Q_0, except for $Q_0 = -(N + 1/2)e$, there exists a smaller, but nonzero, energy level required for the addition or removal of a charge carrier. Under such circumstances, there is no current at low temperatures. However, if $Q_0 = -(N + 1/2)e$, then the state with $Q_0 = -Ne$ and the state with $Q_0 = -(N + 1)e$ are degenerate, and the charge varies between these two values even at zero temperature. Hence, the energy gap in the tunneling spectrum disappears and the current can flow (Fig. 14b). Conductivity peaks appear when the condition $C_gU_g = Q_0 = -(N + 1/2)e$ is satisfied. These peaks are periodic and are separated by a gate voltage equal to e/C_g (Fig. 13a).

Thus, the energy gap in the tunneling spectrum exists for all Ug except for the points of charge degeneracy (Figs. 13a, 14b). Closer discrete levels, shown outside this energy gap, exist due to the excited states of the charge carriers in the QD. When U_g continuously grows, the energy gap shifts downwards with respect to the Fermi energy until it reaches the point of charge degeneracy. When the gap crosses this point, the tunneling spectrum changes abruptly: the energy gap disappears and then appears again with an upward shift of e^2/C. At the same time, the charge of the QD increases by e and the process is repeated. The point of charge degeneracy and the conductivity peak are reached each time the voltage increases by e/C_g; moreover, this value is necessary for addition of one charge carrier to the QD.

It should be noted that the model of the Coulomb blockade takes the charge quantization into account but disregards the energy quantization that arises due to the small size of the QD. At low energies, the confinement makes the distances between the energy levels in the QD relatively large. Taking the confinement into account somewhat changes the pattern of Coulomb recharging of the QD [3, 8, 32]. In particular, the Coulomb oscillations become aperiodic as the number of charge carriers in the QD decreases. Therefore, in relation to tunneling through a few-electron dot, the distance between the two neighboring peaks is

$$\Delta U_g = \frac{e}{C} + \frac{\varepsilon_{N+1} - \varepsilon_N}{e} \quad (4)$$

thus, this distance depends on the peak number, in contrast to the case of many-electron dots, for which the Coulomb oscillations are strictly periodic (Fig. 13a). To calculate the positions of the peaks of the Coulomb oscillations more accurately, we have to numerically calculate the energy eigenvalues for the real shapes of the QDs [12, 34].

The energy spectrum of a QD can also be investigated by measuring the dependence of the tunneling current on the voltage U_{ds} at fixed values of U_g (Fig. 13b), e.g., at those that satisfy the condition $Q_0 = -(N + 1/4)e$. In this case, the Fermi level of the source is raised with respect to its position in the drain, according to the increase in U_{ds}. Furthermore, the Fermi level E_F rises with respect to the confinement levels (Fig. 14c). The current begins to flow as soon as the Fermi level of the source rises above the first confinement level. When the Fermi level rises further, the higher energy levels begin to contribute to the current. The positions of the confinement levels can be determined from the conductivity curves corresponding to the Coulomb staircase (Fig. 13b)

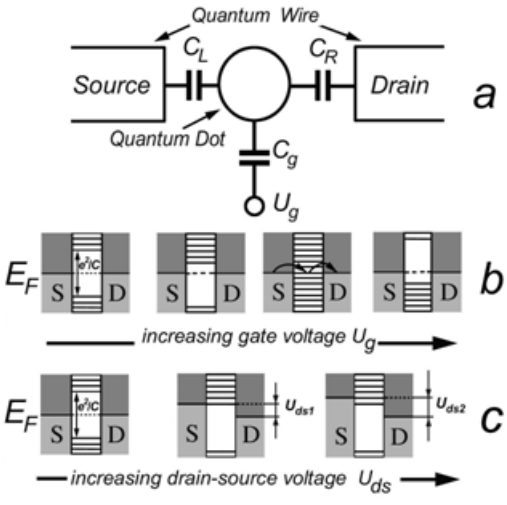

Fig. 14. (a) An equivalent circuit for a weakly coupled quantum dot inside a quantum wire with an applied gate voltage U_g. The circuit corresponds to a single charge-carrier transistor circuit. (b, c) A band diagram of a quantum dot in relation to the charge state and charge-carrier kinetic energy, which can be adjusted by changing (b) the gate voltage U_g and (c) the source–drain voltage U_{ds}.

by measuring the voltages at which the current increases or, equivalently, the voltages corresponding to the peaks in the dI/dU_{ds} curve [6, 8]. At high U_{ds}, the second, third, etc. confinement levels are seen (Fig. 13b). Furthermore, the confinement levels are shifted by eU_g as the voltage U_g increases. It will be shown below that these shifts result in the corresponding asymmetry of the curves $I = f(U_{ds})$ and dI/dU_{ds}.

Thus, the Coulomb blockade mode is characterized not only by the fact that the condition $kT < e^2/2C$ is satisfied but also by the appearance of periodic Coulomb peaks that originate from the one-electron recharging of a QD. The values of the conductivity, even at the maxima of the Coulomb peaks, are much smaller than the conductivity quantum e^2/h [35–37].

3.2 Local tunneling spectroscopy of many-hole silicon QDs in the Coulomb blockade mode

The technique of local tunneling spectroscopy is based on the use of a scanning tunneling microscope (STM). In this study, we used an STM with an electromagnetic system characterized by a rough approach of the tip to the sample in the temperature range 4.2–300 K. Using this technique, the largest area that could be scanned at 300 K was 4 x 4 μm^2 and the largest area at 4.2 K was 0.6 x 0.6 μm^2. The STM measurements were performed using mechanically sharpened steel and tungsten tips. Local tunneling current–voltage curves $I = f(U_{tunn})$ were recorded at T = 4.2 and 300 K during study of the processes involved in the transport of individual holes in the SASQWSs described above. The tunneling current was measured as a function of the voltage applied between the STM tip and the contacts at the boundaries of the planar structure formed in the Hall geometry (Fig. 2a).

Figures 15, 16, and 17 show the tunneling current–voltage characteristics that correspond to different points of the boron diffusion profile in the Si (100) surface representing a δ-shaped barrier under which the SASQWSs are located. Although the local tunneling curves are appreciably different, all of them show the presence of Coulomb interaction and quantum confinement effects in the transport of individual holes in the QWrs, which are induced electrostatically in some regions of the SASQWSs by voltage Utunn being applied between the STM tip and the contact at the boundary of the planar structure (Fig. 2a). As was noted above, these QWrs appear due to the electrostatic ordering of impurity dipoles in the δ barriers. This ordering is induced by the STM tip as it approaches the surface of the diffusion profile. The orientation of the QWrs is determined by the relative positions of the tip and the contact at the boundary of the planar structure.

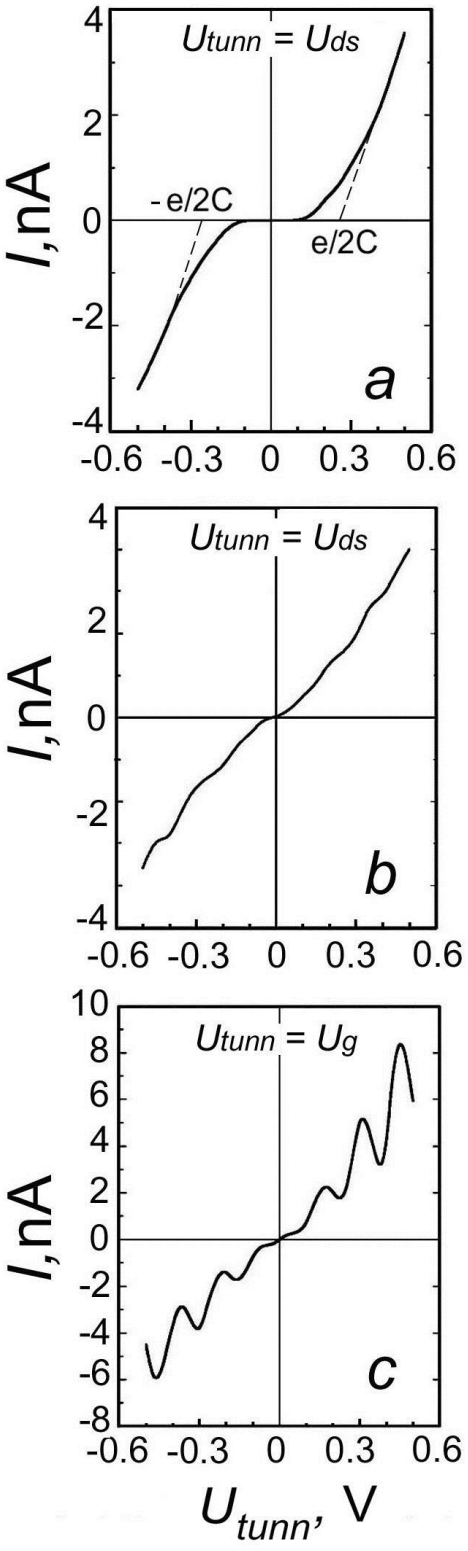

Fig. 15. Local tunneling current–voltage characteristics showing (a) the Coulomb blockade, (b) the confinement effect, and (c) Coulomb oscillations at the transit of individual holes through a weakly coupled many-hole silicon dot inside a *p*-type SASQWS at the Si (100) surface (T = 4.2 K).

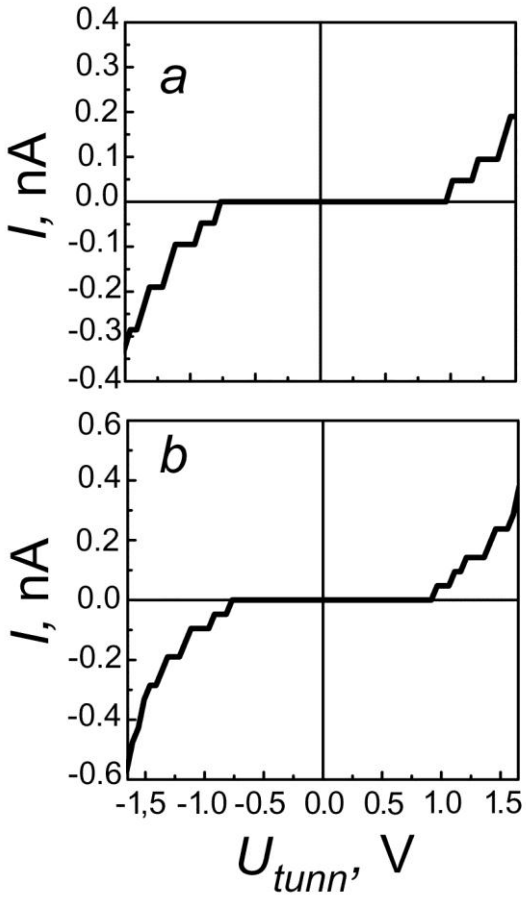

Fig. 16. Local tunneling current–voltage characteristics corresponding to the mode of the Coulomb blockade at the gate voltages U_g (a) 0.7–1 and (b) 0.6–0.9 V. The blockade arises at the transit of individual holes through a weakly coupled many-hole quantum dot inside a *p*-type SASQWS at the Si (100) surface (T = 300 K).

The current and the shape of the local current–voltage characteristic depend on the mode of the ballistic transport of individual holes. The main characteristics of the QWr responsible for the shape of the local current–voltage curves are its smoothness, which varies due to fluctuations in the distribution of the alloying impurity, and the presence of isolated QDs. Furthermore, it is important how close these QDs are to the region where the tip directly affects the surface of the diffusion profile (Figs. 2b, 2c). This closeness determines the voltage drop across a QD, which is equivalent to the gate voltage Ug in a circuit with a field-effect transistor. If an isolated QD formed inside a dynamic QWr is located outside the region of the direct effect of the tip, then $U_{tunn} = U_{ds}$. However, when the tip is close to a zero-dimensional defect, we have $U_{tunn} = U_g$. Hence, the local tunneling current–voltage curves (see Figs. 15, 16, 17) that characterize the transport of individual carriers in electrostatically induced Qrs are representative of the standard $I_{ds} = f(U_{ds})$ and $I = f(U_g)$ curves for a single-electron transistor (see Figs. 13b, 13c).

The shape of the local tunneling current–voltage characteristics shown in Figs. 15a, 16a, and 16b corresponds to the mode of the Coulomb blockade, which arises due to the presence a weakly coupled many-hole QD inside a QWr. These I–V curves are indicative of the charge quantization that leads to an energy gap in the spectrum of states for charge carrier tunneling through a QD (Fig. 14b).

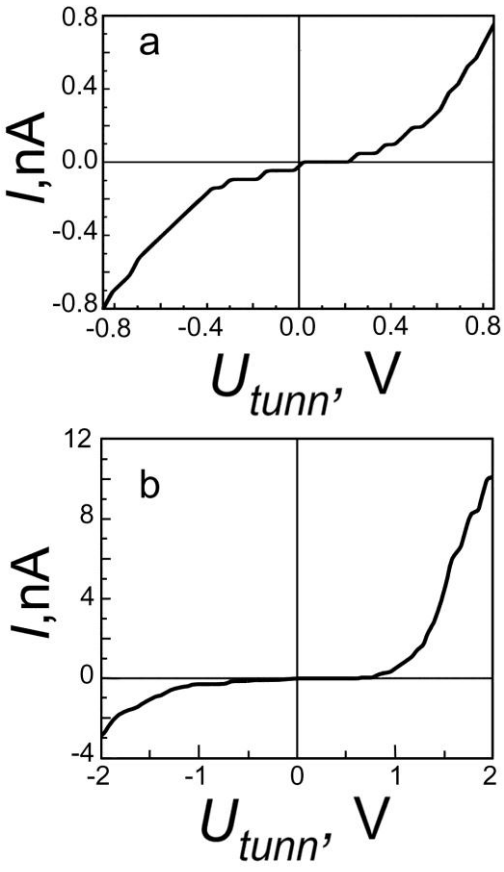

Fig. 17. Local tunneling current–voltage characteristics showing (a) the effect of quantum confinement at the transit of individual holes through a weakly coupled many-hole quantum dot inside a *p*-type SASQWS at the Si (100) surface (T = 330 K) and (b) the different modes of Coulomb blockade at $U_{tunn} > 0$ and $U_{tunn} < 0$ resulting from the asymmetry in the location of a weakly coupled many-hole quantum dot between the microscope tip and the contact at the periphery of the planar structure (T = 300 K).

According to the model of the Coulomb blockade, for an electron to tunnel through a QD, the electron thermal energy (kT) and kinetic energy (eU_{tunn}) must exceed the Fermi energy by $e^2/2C$. Accordingly, the hole energy must be lower than the Fermi energy by the same quantity. When measuring local current–voltage characteristics, the threshold voltage for overcoming the Coulomb blockade is determined by the hole kinetic energy ($U_{tunn} > e/2C$). For the structures under study, this voltage is 0.15 and 1.0V, respectively, both in the forward and reverse current–voltage characteristics. These values correspond to the QD capacitance values of 5×10^{-19} and 8×10^{-20} F. Thus, the parameters of the structures under consideration indicate that the Coulomb blockade can be observed at room temperature, as was demonstrated virtually for the first time when studying the recharging of silicon many-hole QDs (Fig. 16a). The result obtained is probably related to the complicated connecting structure of the QDs, which takes the form chains of multi tunneling silicon junctions (Figs. 2b, 2c) separated by high-energy barriers. In this case, the total capacitance of the QDs decreases, since a QD itself is a series connection of QDs. As the above current–voltage curves are symmetric with respect to zero applied voltage, a QWr contains at least two tunneling barriers and the main part of the applied voltage drops across these barriers. Under the conditions of the Coulomb blockade, these barriers, between which the QDs are localized, have different widths, which can be electrostatically tuned depending on the direction of the applied voltage, as is indicated by the symmetry of the forward and reverse current–voltage characteristics with respect to zero applied voltage. The similar behavior of the *I–V* curves indicates that the voltage applied between the STM tip and the contact at the boundary of the planar structure corresponds to the source–drain voltage $U_{tunn} = U_{ds}$, since a QD is located virtually in the middle of the dynamic QWr containing it. However, the situation is different if we consider the local *I–V* curve in Fig. 17b, obtained at an asymmetric location of a QD with respect to the ends of the electrostatically induced QWr containing it (this curve shows the effect of the Coulomb blockade only for the forward current–voltage characteristic). We can see that, in this case, the barrier width is not an electrostatically tuned parameter.

In Figs. 15b and 17a, we can see current–voltage curves of a different type. These curves exhibit features in the shape of steps symmetrically located with respect to $U_{ds} = 0$, both at positive and at negative applied voltages U_{ds}. The appearance of steps in the $I = f(U_{tunn})$ curves can be explained using the above model of Coulomb oscillations, which are seen against a background of Coulomb blockade if we take the confinement effect into account. In other words, the $I = f(U_{tunn})$ curves seem to represent the spectra of the confinement energy levels in QDs.

As U_{ds} increases, the Fermi level of the source (tip) rises with respect to its position in the drain (an ohmic contact to the sample) and, therefore, with respect to the confinement levels. The current starts to flow as the Fermi level of the source crosses a confinement level (Fig. 14c). At a further rise in the Fermi level, the higher confinement levels contribute to the current, thus producing its stepped growth (Figs. 15b, 17a). Therefore, the positions of the steps in Figs. 15b and 17a are determined by the energies of the confinement levels, which are pinned to the levels of charge quantization (Fig. 14c). Furthermore, the presence of Coulomb steps in the local current–voltage curves indicates that, in the specific geometry of the experiment, the isolated dots are located outside the range of the direct effect of the STM tip ($U_{tunn} = U_{ds}$).

IV. FEW-ELECTRON ARTIFICIAL ATOMS

4.1. The formation of electronic shells

At low temperatures, few-electron QDs show a discrete energy spectrum with a characteristic gap between the confinement levels. In order of magnitude, this gap is comparable to the energy of the Coulomb interaction. In this case, the energy (U) required for placing an electron onto a QD is essentially similar to the electronic affinity of a real atom. In the presence of a limited number of charge carriers in a QD, low energy excitations can transfer the carriers to higher confinement levels. Due to the Coulomb interaction between the charge carriers, the energy corresponding to these excitations is much smaller than U.

Thus, we can draw a parallel between charged few electron QDs and real atoms; however, there are two fundamental distinctions. In real atoms, the Coulomb field has a spherical symmetry and is quantized in units of the elementary charge because of the discreteness of the nucleus charge. It should be noted that, in a real atom, the spectrum of energies corresponding to the addition or removal of an electron can only be weakly controlled. The electrons in a real atom interact with a fixed nucleus potential and with each other, and these two interactions determine the energy spectrum. At the same time, the Coulomb field in a QD may have an arbitrary symmetry and vary continuously (with respect to the elementary charge). Thus, it is possible to totally change the energy spectrum of an artificial atom by changing its geometry or structure [12, 34].

When filling the discrete energy levels in highly symmetric QDs by electrons, the effects of orbital

degeneracy and the formation of shells characteristic of real atoms can appear. We recall that the presence of a 3D spherically symmetric potential in an atom results in the appearance of a shell structure with 1*s*, 2*s*, 2*p*, … shells. The ionization energy is at its highest for atomic numbers 2, 10, 18, …, and, up to the atomic number 23, these shells are filled sequentially according to Hund's rule. Therefore, the filling of the corresponding shells in the QDs must also depend primarily on factors such as electron–electron interaction and electron spin [12].

The identification of the electronic shells of QDs has become possible due to the use of scanning tunneling microscopy (STM). A study of the local tunneling current–voltage characteristics of separate semiconductor nanocrystalline InAs QDs, which had a characteristic size ranging from 2 to 8 nm, made it possible to show that, in particular, the first and second excited states of the conduction band had the *s* and *p* symmetry manifesting itself in the corresponding multiplet series [13].

4.2 Local Tunneling Current–Voltage Characteristics of Few-Electron Silicon QDs

Local tunneling $I = f(U_{tunn})$ curves, which represent the energy spectra of QDs, are a particularly effective tool for identification of the parameters of few-electron silicon QDs. In this study, we present the results of studies of few-electron small-size silicon artificial atoms for the first time. These results make it possible to determine the positions of the confinement levels, even at room temperature, using local tunneling spectroscopy data.

Figures 18–20 show the current–voltage characteristics obtained for the electron transit through QDs located in p-type longitudinal SASQWSs with a built in longitudinal component in the field of the p+–n junction [38]. As a result of this configuration, the QD conduction can be locally inverted from *p*-type to *n*-type. These current–voltage characteristics show that, due to their small size, the few-electron QDs under study have a discrete energy spectrum with a characteristic separation between their confinement levels; in order of magnitude, this separation is comparable to the energy of the Coulomb interaction. In particular, the conductance of high-symmetry dots with a characteristic size of ~2 nm (Fig. 1c) is obviously indicative of the s and p symmetry manifested in the corresponding local tunneling *I–V* curves by the series of multiplets (Fig. 18). In other words, when filling discrete energy levels in high-symmetry few-electron QDs with electrons, orbital degeneracy and shell formation specific to real atoms are observed. The effect of the formation of electronic shells appeared to be very sensitive to the local electric fields and virtually completely disappeared both as the STM tip approached a few-electron QD and as its symmetry was disrupted by local fluctuations in the boron distribution in the δ barriers (Fig. 19). It is interesting that, in spite of the suppression of the formation of electronic shells, the energy gaps between the confinement levels are conserved (Fig. 19) and, in addition, in some cases, their spin degeneracy is removed (Fig. 20).

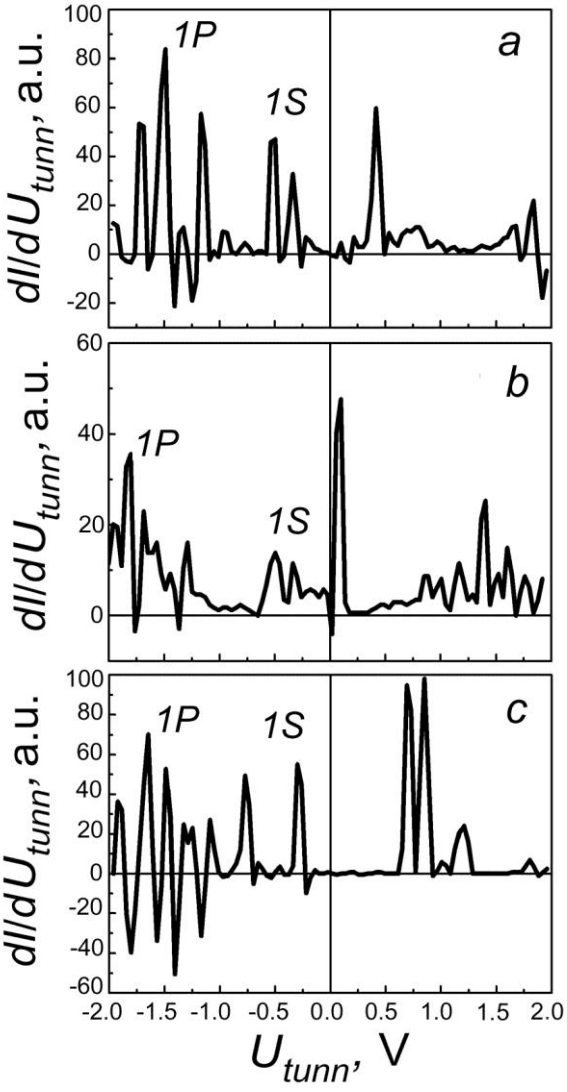

Fig. 18. The conductance of a strongly coupled few-electron quantum dot inside an SASQWS on the Si (100) surface at T = 300 K. Spectra (a), (b), and (c) are measured at different positions of the STM tip with respect to the QD and indicate the formation of electronic shells.

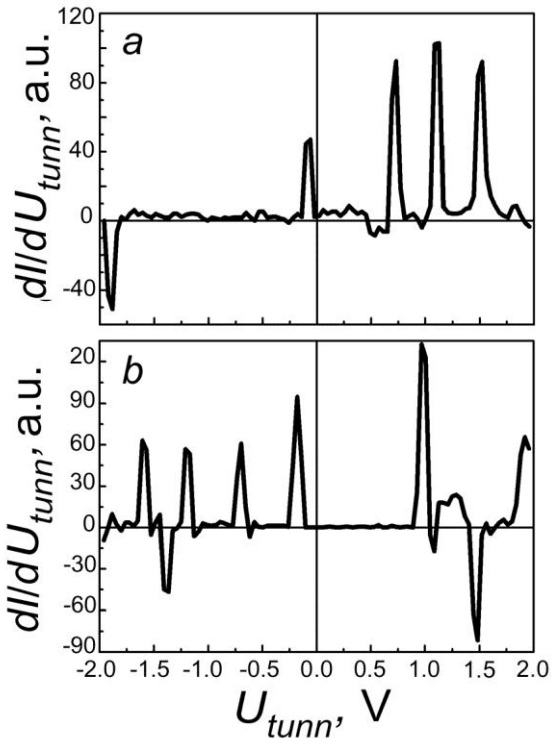

Fig. 19. The conductance of a strongly coupled few-electron QD inside an SASQWS on the Si (100) surface at T = 300 K. Spectra (a) and (b) are measured at different positions of the STM tip near the QD and indicate the suppression of the formation of electronic shells, which results from the closeness of the STM tip to the QD.

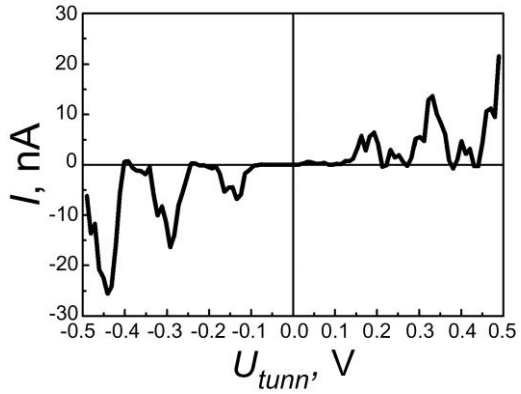

Fig. 20. A local tunneling current–voltage characteristic indicating the Coulomb oscillations under the conditions of removal of the spin degeneracy of the quantum confinement levels at the transit of individual electrons through a weakly coupled few-electron quantum dot inside an SASQWS at the Si (100) surface (T = 4.2 K).

V. CONCLUSION

Short-time boron diffusion has been realized into monocrystalline silicon through controlled surface injection of self-interstitials and vacancies by varying the diffusion temperature and the parameters of the oxide overlayer on the Si(100) wafer. Space-independent excess fluxes of intrinsic defects that are induced by the deformed potential fluctuations near the Si-SiO2 interface have permitted ultra-shallow diffusion profiles which consist of self-assembled longitudinal and lateral heavily doped quantum wells (SASQWSs). The microdefects of the self-interstitials type that are formed inside such profiles by the diffusion process of boron have been demonstrated to promote the realization of self-assembled silicon superlattices and microcavities.

The local tunneling spectroscopy studies have shown that, in the SASQWSs at the surface of Si (100), the STM tip induces quantum wires (QWrs) with many-hole weakly coupled quantum dots (QDs) and few-electron strongly coupled QDs.

Local tunneling current–voltage characteristics show the different modes of Coulomb blockade and Coulomb conductivity oscillations occurring at the transit of single holes through many-hole weakly coupled QDs. The manifestation of these modes is caused by the Coulomb interaction and quantum confinement effects.

It is shown that, for tunneling through many-hole QDs, the Coulomb oscillations have a periodic character, whereas, for the transport through few-electron dots, the regularity of the oscillations is disrupted.

The local tunneling current–voltage characteristics of high-symmetry few-electron silicon QDs indicate the formation of shells specific to real atoms.

ACKNOWLEDGEMENTS

Authors acknowledge the support of the Presidium of the Russian Academy of Sciences, program “Topical Problems of Low-Temperature Physics”, grant no. 10.4, project no. 10.17, the support of Ioffe Institute, Russian Academy of Sciences and the support of the Department of Science and Higher Education of the St. Petersburg government. The study was supported in part by the Ioffe Institute, Russian Academy of Sciences.

REFERENCES

[1]. C. Weisbuch and B. Winter. *Quantum semiconductor structures* (N.Y.: Academic Press, 1991).
[2]. T.J. Thornton, Mesoscopic devices, *Rep. Progr. Phys., 58,* 1994, 311-364.
[3]. C.G. Smith, Low-dimensional quantum devices, *Rep. Progr. Phys., 59*, 1996, 235-282.
[4]. N.N. Ledentsov, Ordered arrays of quantum dots, *Proc. of 23th Int. Conf. on the Phys. of Semicond.,* Berlin, Germany, 1996, 19-26.

[5]. L. Eaves, Magnetotunneling spectroscopy of quantum wells, wires, dots and chaotic stadia, *Proc. of 23th Int. Conf. on the Phys. of Semicond.*, Berlin, Germany, 1996, 43-50.
[6]. M.A. Kastner, Artificial atoms, *Physics Today*, *46*, 1993, 24-31.
[7]. R. Nötzel, Self-organized growth of quatum-dot structures, *Semicond. Sci. Technol*., *11*, 1996, 1365-1369.
[8]. U. Meirav and E.B. Foxman, Single electron phenomena in semiconductors, *Semicond. Sci. Technol., 10*, 1995, 255-284.
[9]. S.L. Feng and J.C. Bourgoin, DX centers in superlattices, *Sol. St. Phenomena., 10*, 1989, 265-272.
[10]. N.T. Bagraev, A.D. Bouravleuv, L.E. Klyachkin, A.M. Malyarenko, W. Gehlhoff, V.K. Ivanov and I.A. Shelykh, Quantized conductance in silicon quantum wires, *Semiconductors, 36*, 2002, 439-460.
[11]. C.T. Liang, M.Y. Simmons, S.G. Smith, G.H. Kim, D.A. Ritchie and M. Pepper, Experrimental evidence for Coulomb charging effects in a open dot at zero magnetic field, *Phys. Rev. Lett., 81*, 1998, 3507-3510.
[12]. S. Tarucha, D.G. Austing and T. Honda, Shell filling and spin effect in a few electron quantum dot, *Phys.Rev.Lett., 77*, 1996, 3613-3616.
[13]. O. Millo, D. Katz, Y. Levi, Y.W. Cao and U. Banin, Size-dependent tunneling and optical spectroskopy of InAs nanocrystal quantum dots, *J. Low Temp. Phys., 118*, 2000, 365-374.
[14]. D. Goldhaber-Gordon, Hadas Shtrikman, D. Mahalu, David Abush-Magder, U. Meirav and M.A. Kastner, Kondo effect in a single-electron transistor, *Nature, 391*, 1998, 156-159.
[15]. J. Göres, D. Goldhaber-Gordon, S. Heemeyer, M.A. Kastner, Hadas Shtrikman, D. Malahu and U. Meirav, Fano resonances in electronic transport through a single-electron transistor, *Phys.Rev.B, 62*, 2000, 2188-2194.
[16]. U. Gosele and T.Y.Tan, Point defects and diffusion in silicon and gallium arsenide, *Def. Diff. Forum, 59*, 1988, 1-15.
[17]. N.T. Bagraev, L.E. Klyachkin, A.M. Malyarenko and V.L. Sukhanov, Quantum-Size p-n Junctions in Silicon, *Solid State Electronics, 34*, 1991, 1149-1156.
[18]. N.T. Bagraev, A.D. Bouravleuv, W. Gehlhoff, L.E. Klyachkin, A.M. Malyarenko and S.A. Rykov, Self-assembled impurity superlattices and microcavities in silicon, *Def. Diff. Forum, 194-199*, 2001, 673-684.
[19]. J. Robertson, Electronic structure of amorphous semiconductors, *Adv. in Phys*., *32*, 1983, 361-452.
[20]. E.H. Poindexter, P.J. Caplan, B.E. Deal and G.J. Gerardy, Chemical and Structural Features of Inherent and Process-Induced Defects in Oxidized Silicon, in: B.E. Deal and C.R. Helms, (Eds.), *The Physics and Chemistry of SiO_2 and Si-SiO_2 Interface* (New York: Plenum Press, 1988) 299-308.
[21]. N.T. Bagraev, A.D. Bouravleuv, W. Gehlhoff, L.E. Klyachkin, A.M. Malyarenko, V.V. Romanov and S.A. Rykov, Fractal self-assembled nanostructures on monocrystalline silicon surface, *Def. Diff. Forum, 237-240*, 2005, 1049-1054.
[22]. P.S. Zalm, Ultra shallow doping profiling with SIMS, *Rep. Progr. Phys., 58*, 1995, 1321-1374.
[23]. W. Gehlhoff, N.T. Bagraev and L.E. Klyachkin, Shallow and deep centers in heavily doped silicon quantum wells, *Mater. Sci. Forum, 196-201*, 1995, 467-472.
[24]. Bao-xing Li, Pei-lin Cao, and Duan-lin Que, Distorted icosahedral cage structure of Si_{60} clusters, *Phys.Rev.B, 61*, 2000**,** 1685-1687.
[25]. R. Houdré, R. P. Stanley, U. Oesterle, M. Ilegems, and C. Weisbuch, Room-temperature cavity polaritons in a semiconductor microcavity, *Phys.Rev.B, 49*, 1994, 16761-16764.
[26]. W. Gehlhoff, N.T. Bagraev and L.E. Klyachkin, Cyclotron resonance in heavily doped silicon quantum wells, *Sol. St. Phenomena, 47-48*, 1995, 589-594.
[27]. N.T. Bagraev, W. Gehlhoff, L.E. Klyachkin, A.M. Malyarenko and A. Näser, Spin-dependent processes in self-assembly impurity quantum wires, *Mater. Sci. Forum, 258-263*, 1997, 1683-1688.
[28]. N.T. Bagraev, L.E. Klyachkin, A.M. Malyarenko, E.I. Chaikina, E.V. Vladimirskaya, V.E. Gasumyants, V.I. Kaidanov, V.V. Kveder and A.I. Shalynin, Metal-insulator transition in strongly doped p^+ quantum wells on a n-type silicon surface, *Semiconductors, 29(12)*, 1995, 1112-1124.
[29]. N.T. Bagraev and V.A. Mashkov, A mechanism for two-electron capture at deep level defects in semiconductors, *Sol. St. Commun., 65*, 1988, 1111-1117.
[30]. N. T. Bagraev, Zn-Related Center in Silicon: Negative-U Properties, *J. Phys. (France) I, 2*, 1992, 1907.
[31]. N.T. Bagraev, W. Gehlhoff, V.K. Ivanov, L.E. Klyachkin, A.M. Malyarenko and I.A. Shelykh, Interference of Ballistic Carriers in Modulated Quantum Wires, *Phys.Low-Dim.Struct., 1/2*, 2000, 37-48.
[32]. D.V. Averin, A.N. Korotkov, and K.K. Likharev, Theory of single-electron charging of quantum wells and dots *Phys.Rev. B, 44*, 1991, 6199-6211.
[33]. H. van Houten and C.W.J. Beenakker, Comment on ‘‘Conductance oscillations periodic in the density of a one-dimensional electron gas’’, *Phys. Rev. Lett. 63*, 1989, 1893-1897.
[34]. Satyadev Nagaraja, Philippe Matagne, Voon-Yew Thean, Jean-Pierre Leburton, Yong-Hoon Kim, and Richard M. Martin, Shell-filling effects and Coulomb degeneracy in planar quantum-dot structures, *Phys. Rev. B 56*, 1997, 15752-15759.
[35]. L.I. Glazman and M.E. Raikh, Resonant Kondo transparency of a barrier with quasilocal impurity states, *JETP Lett. 47*, 1988, 452-455.
[36]. L.I. Glazman and K.A. Matveev, Lifting of the Coulomb blockade of one-electron tunneling by quantum fluctuations, *JETP 71*, 1990, 1031-1037.
[37]. M. Tewordt, V.J. Law, J.T. Nicholls, L.Martín-Moreno, D.A. Ritchie, M.J. Kelly, M. Pepper, J.E.F. Frost, R. Newbury and G.A.C. Jones, Single-electron tunneling and Coulomb charging effects in ultrasmall double-barrier

heterostructures, *Solid-State Electron., 37*, 1994, 793-799.

[38]. N.T. Bagraev, A.D. Bouravleuv, W. Gehlhoff, L.E. Klyachkin and A.M. Malyarenko, White light emission from nanostructures embedded in ultra-shallow silicon p-n junctions, *Proc. of the 26th International Conference on the Physics of Semiconductors*, Edinburgh, U.K., 2002, G3.3.

N.T. Bagraev." Single-Hole Charging in Self-Assembled Silicon Nanostructures" "International Journal of Engineering Research and Applications (IJERA), vol. 8, no. 2, 2018, pp. 50-66.